Wideband Hybrid Precoding Techniques for THz Massive MIMO in 6G Indoor Network Deployment

Jeyakumar P (jeyakumarpsg@gmail.com)
National Institute of Technology Tiruchirappalli https://orcid.org/0000-0002-2043-790X
Vishnu V
National Institute of Technology Tiruchirappalli
Srinitha S
Sri Ramakrishna Engineering College
Muthuchuchidambaranathan P
National Institute of Technology Tiruchirappalli
Arvind Ramesh
National Institute of Technology Tiruchirappalli

Research Article

Keywords: Terahertz, Delay-phase Precoding, Beam Spilt effect, 6G Indoor Office, Channel Simulation

Posted Date: July 9th, 2021

DOI: https://doi.org/10.21203/rs.3.rs-568831/v1

Noname manuscript No.
(will be inserted by the editor)

Wideband Hybrid Precoding Techniques for THz Massive MIMO in 6G Indoor Network Deployment

Jeyakumar P[1], Vishnu V[2], Srinitha S[2], Muthuchidambaranathan P[1],Arvind Ramesh[1]

Received: date / Accepted: date

Abstract Terahertz (THz) communication is becoming an up-and-coming technology for the future 6G networks as it provides an ultra-wide bandwidth. Appropriate channel models and precoding techniques are essential for supporting the desired coverage and mainly to resolve the severe path loss in THz signals. Initially, the Sub-THz channel (140 GHz) impulse response by using NYUSIM Channel Simulator for 6G indoor office scenario is investigated in this work. The highlight is on Large scale and Small scale parameters like propagation delay and path loss, antenna array gain, etc. The beam split effect is a critical challenge of THz wideband communication.Therefore We have proposed three different THz precoding methodologies like the hybrid precoding, analog beamforming, and the delay-phase precoding to address this challenge.

Jeyakumar P[1]
Department of Electronics and Communication Engineering,
National Institute of Technology, Tiruchirappalli 620015,India
E-mail: jeyakumarpsg@gmail.com

Vishnu V[2]
Department of Electronics and Communication Engineering,
National Institute of Technology, Tiruchirappalli 620015,India
E-mail: vishnuv0209@gmail.com

Srinitha S[2]
Department of Electronics and Communication Engineering,
Sri Ramakrishna College of Engineering, Coimbatore, India
E-mail: srinitha@srec.ac.in

Muthuchidambaranathan P[1]
Department of Electronics and Communication Engineering,
National Institute of Technology, Tiruchirappalli 620015,India
E-mail: muthuc@nitt.edu

Arvind Ramesh[1]
Department of Instrumentation and Control Engineering,
National Institute of Technology, Tiruchirappalli 620015,India
E-mail: arvindramesh25@gmail.com

We then extensively investigate its diverse number of time delayers, varying number of antenna elements, and comparison with frequency - mmWave and Sub-THz have been discussed. Finally, the proposed delay-phase precoding techniques outperforms the other precoding techniques with 97% of optimal precoding. So, this an efficient approach for implementing the future indoor communication network deployment for 6G.

Keywords Terahertz, Delay-phase Precoding, Beam Spilt effect, 6G Indoor Office, Channel Simulation

1 Introduction

The International Tele-communication Union(ITU) launched the official research investigation over 6G helps to design pioneer wireless networks and also to attain self-subsisting networks. To quench out the emerging services and the applications like augmented reality, holographic communications, extremely high definition transmission of videos, the Tera-Hertz(THz) communications acts as a backbone for the future 6G wireless networks. 6G also provides the communication with reduced latency for long distance with ultra high reliability. The THz band ranges from 0.1THz to 10THz provides significant bandwidth owing to attain ultra-high data rate. Several interpretations over 6G be has a belief that 6G provides an empowered full-dimensional coverage with unlimited wireless connectivity.

For wireless communications, the peak data rate is considered to be an essential indicator to measure its effectiveness and in order to accomplish the above visions of 6G, the peak data rate should be greater than 1 Tbps [1], [2]. Nevertheless, this peak data rate will not be supported by the existing 5G millimeter wave (mmWave) bandwidth. Comparing THz band, which is in 0.1 THz-10 THz range with the mmWave, the THz band provides the significant bandwidth, for example, the bandwidth greater than 20 GHz is provided to accomplish the extremely high data rate. Therefore, it is extensively believed that the communication through THz band is significant technology for the emerging 6G wireless networks [2]. The bandwidth provided should be used effectively in multi-user networks. An autonomous and large dimensional networks are the key features of 6G to provide wide coverage and ubiquitous connectivity.

The bandwidth obtained in the sub 6 GHz of band, and the mmWave band is insubstantial to gratify the exigencies of the users in sixth generation era. The usage of available spectrum is started moving towards the THz band in bandwidth hungry applications [3]. In the applications of cellular, biological, molecular and vehicular communications, distinct use cases are encountered [4-6]. Owing to the bottleneck of large path loss, the THz communication is circumscribed to employ in short range applications. A good number of advanced applications like personal area networks, 6G communication, chip to chip communication uses THz band communication [7].

But the THz signals are often affected by the path loss for example, at 0.6 THz the path loss of 120 dB/100 m will occur. Due to this path loss issue it becomes challenging to accomplish the expected coverage. The precoding approach helps to resolve path loss problem and in this approach there is no need to increase the power at the transmitter. By using this precoding methodology, narrow beams can be generated with large antenna array gain that combats the severe path loss and also the entire optimization process will be simplified into sub rate optimization processes and its complexity is evaluated [8].

The scale of the antenna array is directly proportional to the array gain of the emerging beam. The wavelength of the signal obtained from the THz band is considerably very small, therefore in THz communication, antenna arrays of very large scale is employed. As the optimization of path loss of THz signals can be used by THz precoding, which is a requisite methodology for 6G wireless networks. When compared to the precoding approach used in 5G mmWave systems, the 6G precoding techniques is facing new challenges because of its varied characteristics and these challenges should detected and resolved by an effective 6G system.

The major bottleneck of current wireless communication system is the limitation of available spectrum and because of that the significant quality of service cannot be provided and this can be alleviated by adopting the THz communication. The spectrum gridlock can be removed by applying novel methodologies and new frequency bands. For effective THz communication, the array-of-sub-array architecture is compared with the fully connected architecture. The comparison is made in terms of energy efficiency, spectral efficiency, power consumption, channel estimation etc., Highly complex and power consuming hardware is required for THz communication and many new communication strategies are applied owing to the nature of hardware [9]. In order to realize a wireless backhaul with an ultra-high speed, it is vital to analyze the bandwidth, transmission distance and the physical properties of the channel. To address these challenges in THz band, the distance can be enhanced by using distance aware bandwidth adaptive methodology. This approach capture all the distinct eccentricities of the channel and uses a full spectrum of resources by enabling several high-speed links. Highly advanced communication methodologies are needed to enhance the distance for transmission and this helps to provide simultaneous operation of ultra high speed links [10].

2 Related work

In 6G networks, an ultra broadband connectivity is offered by mounting the THz access points over the lamp post in the street which helps to provide the better bandwidth availability at the THz frequency range and this also becomes feasible for offloading the traffic from the access point (AP). As high frequencies are bounded by the smallest wavelength, the MIMO configuration

is realized as the user equipment and the access points are outfitted with the arrays that constitutes large number of antenna elements. By using the pertinent beamforming methodology, the pitfall of having higher path loss is overcome by the substantial array gain and the interference caused by multiple users is facilitated by boosting the capacity of the system and to provide beams with high directivity in the massive MIMO configuration [11],[12].

6G networks provides appreciable user throughput but it is also necessary to gratify the system requirements to improve the energy and the spectrum efficiency [13]. These network communication system is also anticipated to perform its operation with cost reduction and limited energy consumption [14]. Depending on the intent of the application, the performance trade offs regarding cost, efficiency and the computation complexity influences the appropriate precoding methodology [15]. Two stages of hybrid precoder constitutes analog beamformer and the digital precoder and these hybrid precoders uses only limited RF chains.

In the traditional hybrid precoding approach, full array gain is achieved by aligning the narrow beam from the analog beamformer in the direction of the intended users [16]. Nevertheless, in 5G mmWave massive MIMO systems, the generated beams from various sub-carrier frequencies concentrate on various physical directions because of the usage of phase shifters which is independent of frequency and this leads to loss in array gain [16]. Various methods are utilized to tackle this array gain loss which is encountered by the beam squint effect [17]–[21]. An optimized closed form solution is proposed in orthogonal frequency division multiplexing to deal with the hybrid precoding problem in the wide band massive MIMO system[18]. To enhance the hybrid precoding approach performance, an optimal solution is proposed to optimize the digital precoder and an analog beamformer iteratively in order to attain the significant performance over the whole bandwidth [1].

Additionally, the design of code books which contains beams of wide bandwidth is made in order to mitigate the beam squint effect which causes loss in array gain [20],[21]. The design of wide beams having reduced array gain is attained in each sub-carrier where a semi-definite relaxation methodology is used to enhance the overall antenna array gain over the whole bandwidth [20],[21]. The suggested methods show effectiveness to enhance the rate performance because the beams are squinted slightly and in case of mmWave massive MIMO systems, the loss in array gain is not a major consideration [18]-[21]. But these methods are not highly effective for THz band massive MIMO communication systems. The generated beams obtained at various sub-carrier frequencies decompose into individual physical directions because of the substantial number of antennas and wide bandwidth of THz signal.

The decomposition of different subcarrier beams in different directions is called as beam split and this is the fundamental difference between THz and mmWave beamforming systems. The beam split effect gives each subcarrier in the signal a different direction, where the subcarriers around the center frequency diverge around boresight of the beam. It is inferred that the significant array gain will be attained only on the generated beams around the

central frequency. And the remaining beams suffer from a high loss in array gain. Consequently, the achievable rate is degraded by beam split effect. This can be overcome by using delay-phase precoding in this work[22,23].

2.1 Major Contributions

- The key contribution of this work is to apply the channel model to evaluate the 6G THz Massive MIMO system performance with NYUSIM Channel Simulation to verify the channel model parameters and antenna properties.

- Large scale and Small scale parameters have been discussed for 6G indoor office scenario for 140 GHz operating frequency under UMi LOS environment at 0 dBm Transmit power with coverage of 100 m.

- Three precoding techniques have been investigated to deploy 6G single cell multi-user indoor office scenarios. The beam split effect is one reason behind to propose the delay-phase precoding technique for reducing the array gain loss that occurs.

- Finally, by varying the number of time delayers, frequency (mmWave and Sub-THz), and the number of transmitting antennas in the proposed delay-phase precoding technique, the performances have been compared.

  The paper is structured as Section 3 explains network deployment model with the small scale fading, large scale fading, power delay profile analysis. Section 4 illustrates various precoding methods like hybrid precoding, analog beamforming, delay-phase precoding techniques, and performance evaluation. The design approach is explained under section 5. Section 6 demonstrates simulation results with its inferences. Finally, Section 7 concludes the article.

3 Network deployment Model

Fig. 1 depicts the massive MIMO THz network deployment model. In indoor office scenarios, the major focus will be in the downlink, where the single cell access point (AP) is connected to multiple users. The small scale and large scale fading channel models, the structure of an antenna array, and the power delay profile analysis are discussed in the following subsections using NYUSIM [24].

3.1 Large Scale Fading

With NYUSIM, the expression for Close In (CI) free-space reference distance path loss model having one meter of reference distance with an additional

attenuation caused by diversified atmospheric conditions were applied [26]-[29], and the expression is given as:

$$PL^{CI}(f,d)[dB] = FSPL(f,1m)[dB] + 10nlog_{10}(d) + AT[dB] + \chi_{\sigma}^{CI} \quad (1)$$

, , where d $\geq$ 1m

d represents the three dimensional(3D) receiver-transmitter separation distance, 'f' represents carrier frequency in GHz, where 'n' denotes the path loss exponent and the attenuation term is denoted by AT which is induced by atmosphere, the path loss in free space (dB) is denoted by FSPL(f, 1 m) with one meter of separation between transmitter and receiver at f and χ_{σ}^{CI} represents a Gaussian random variable with zero-mean and standard deviation in dB:

$$FSPL(f,1m)[dB] = 20log_{10}(\frac{4\pi f \times 10^9}{c}) = 20log_{10}(f) + 32.4[dB] \quad (2)$$

where c represents the speed of light in a vacuum and f is the frequency in GHz. The characterisation of AT is given as:

$$AT[dB] = \alpha[dB/m] \times d[m] \quad (3)$$

The attenuation factor (dB/m) is denoted by 'α' at 1 GHz to 100 GHz of frequency, that constitutes the combined effects of attenuation of haze, rain, dry air and water vapor [27]. Here 'd' represents the 3D transmitter-receiver distance of separation in (1).

3.2 Small-Scale Fading

The double-directional channel impulse response (CIR) h_{dir}, in small scale fading, having 'L 'multi-path components for every transmission link will be provided as follows:

$$h_{dir}(t,\phi) = \Sigma_{l=1}^{L} P_{RX,l}.e^{j\varphi_l}.\delta(t-\tau_l).G_{TX}(\phi-\phi_l^{TX}).G_{RX}(\phi-\phi_l^{RX}) \quad (4)$$

Here G_{TX} G_{RX} represents antenna gain at transmission and reception. $P_{RX,l}$,τ_l and ϕ_l denotes the magnitude of received power,propagation time delay and phase in the multi-path components. ϕ represents azimuth angle offset and 't' denotes time. In every multi-path component, ϕ_l^{TX} denotes the angle of departure at the access point and ϕ_l^{RX} represents the angle of arrival for every mobile users (MUs).

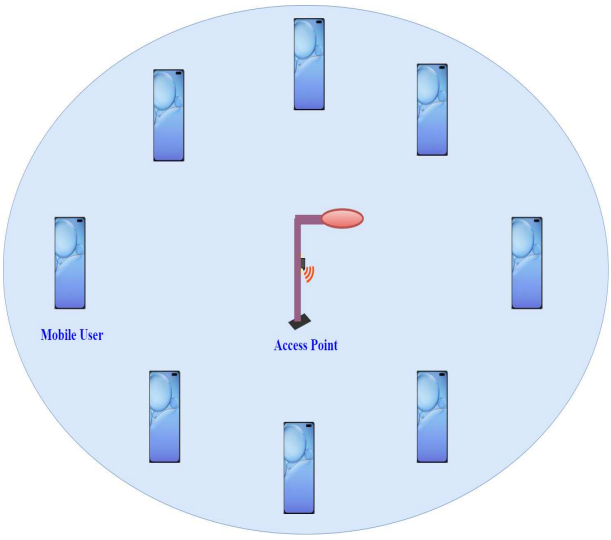

Fig. 1: Network deployment model

3.3 Power Delay Profile Analysis

To create a communication link between the APs and MUs and to maintain the desired data rate of a channel, the received power at the MUs should be modified accordingly. The study of the power delay profile is critical for network deployment. As shown in Table 1, there are a total of 32 input parameters are given as input to the simulator that is categorized into two divisions: antenna properties and channel parameters. The panel antenna properties are made up of 12 input parameters that are linked to the antenna arrays at transmission and reception, while the panel channel parameter is made up of 20 input parameters that provide information on the propagation channel. The proposed network parameters for urban microcell (UMi) indoor THz communication systems are described in Table 1. The APs use a carrier frequency of 0.14 THz and transmit power of 0 dBm[30]. The NYUSIM statistical parameters at 0.14 THz LOS channel path-loss model is given by free space path loss PL_0 = 255.32 dB.

The power spectrum of 3D Angle of Departure (AOD) is shown in Figure 2(a), and the power spectrum of 3D Angle of Arrival(AOA) is shown in Figure 2(b) which have been simulated in NYUSIM. Whereas, the Figure 3(a) depicts the corresponding simulated omni-directional Power delay profile. For the 0.14 THz UMi LOS environment, the separation between transmitter and receiver is held at 100 m. The received power is -122.8 dBm and the path delay σ is 17.9 ns having a Path Loss Exponent (PLE) of 2.4. The directional power delay profile for a 0.14 THz UMi LOS area with a PLE of 2.7 and transmitter and receiver antenna half power beamwidths (HPBW) of 8° azimuth and 8° elevation as shown in Figure 3(b). Both the transmitter and receiver antennas

Table 1: Input parameters settings

Parameters	Value
Frequency(GHz)	140
RF bandwidth(MHz)	1000
Scenario	UMi
Environment	LOS
Lower Bound of T-R Separation Distance(m)	100
Upper Bound of T-R Separation Distance(m)	100
TX Power(dBm)	0
Base Station Height(m)	35
User Terminal Height(m)	1.5
Number of Rx Locations	16
Barometric Pressure (mbar)	1013.25
Humidity(%)	50
Temperature(°C)	20
Rain Rate in mm/hr	0
Polarization	Co-Pol
Foliage Loss	No
Distance within Foliage (m)	0
Foliage Attenuation(dB/m)	0.4
Outdoor to Indoor(O2I) Penetration Loss	No
O2I Loss Type	Low Loss
TX Array Type	ULA
RX Array Type	ULA
Number of TX Antenna Elements (N_t)	256
Number of RX Antenna Elements (N_r)	1
TX Antenna Spacing(in wavelength)	0.5
RX Antenna Spacing(in wavelength)	0.5
Number of TX Antenna Elements Per Row W_t	1
Number of RX Antenna Elements Per Row W_r	1
TX Antenna Azimuth HPBW	8°
TX Antenna Elevation HPBW	8°
RX Antenna Azimuth HPBW	8°
RX Antenna Elevation HPBW	8°

have a gain of 26.5 dBi and the received power is -76.4 dBm with path delay, $\sigma = 0.9$ ns. Figure 4(a) depicts a small scale PDP for indoor deployments with a Tx-Rx separation distance of 100m and a frequency of 0.14 THz. For the Tx and Rx gain of 26.5 dBi, the Path Loss for Omnidirectional, Directional and Directional-best for 0.14 Thz, UMi LOS is shown in Figure 4(b) with respect to Tx-Rx Separation distance.

Throughout this article, the following notations are used: A represents a matrix, 'a' denotes a vector and a is a scalar. A(i) illustrates the ith column of A, (.)* denotes conjugate transpose, $(.)^T$ denotes transpose and tr(A) is its trace. ||A|| is the Frobenius norm of A, and $|A|$ is its determinant; [A | B] represents the horizontal concatenation; The p-norm of a is represented as $||a||_p$; $diag$(A) is a vector generated by the diagonal elements of the matrix A; I_N is the NxN identity matrix; 0_{M*N} is the MxN all-zeros matrix; $n \sim \mathcal{N}(\mu, \sigma^2)$

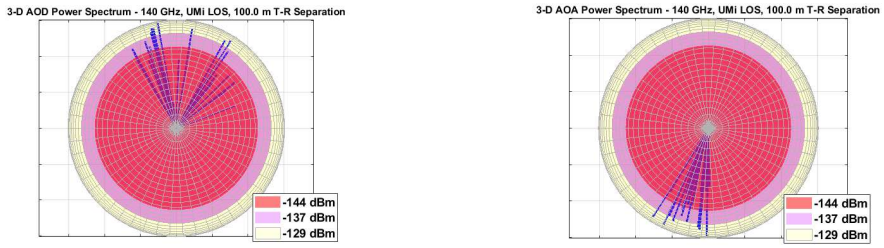

(a) 3D Power Spectrum of AoD (b) 3D Power Spectrum of AoA

Fig. 2: Power Spectrum

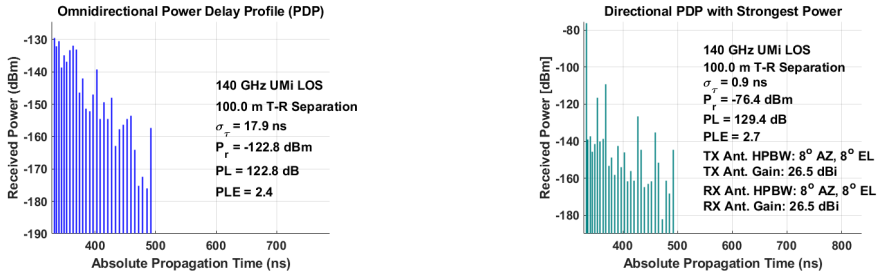

(a) Omnidirectional Power Delay Profile (b) Directional Power Delay Profile

Fig. 3: Power Delay Profiles

is the complex Gaussian vector of covariance σ^2 and mean 0. $E[.]$ denotes the expectation and $R\{.\}$ denotes the real part of the variable.

4 Precoding Techniques

For this precoding, we consider the multi-carrier system, by assuming an AP with N_t antennas and N_{RF} RF chains are communicated via 'M' sub carriers.The sampled transmitted signal is

$$x[m] = F_{RF}F_{BB}[m]s[m], \ for\ m = 1, 2, ..., M, \tag{5}$$

where s $= [s_1, s_2, ..., s_M]^T$ is the $M \times 1$ vector of transmitted symbols, such that $E[s[m]s^*[m]] = \frac{P_t}{M} I_M$, $F_{BB} = [f_1^{BB}, f_2^{BB}, ..., f_M^{BB}]$, $F_{RF} = [f_1^{RF}, f_2^{RF}, ..., f_M^{RF}]$

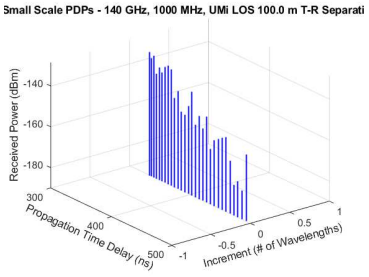

(a) Small Scale Power Delay Profile

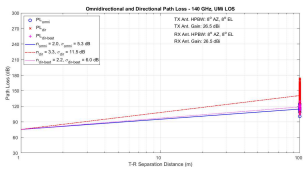

(b) Omnidirectional & Directional Path Loss

Fig. 4: Small scale PDPs & Path Loss

and P_t represents the average total transmitted power. In the time domain, the analog RF precoding (F_{RF}) is performed and for the whole bandwidth, this same precoding matrix is employed. In the frequency domain, the digital baseband precoding ($F^{BB}[m]$) is performed that is based on a per-subcarrier basis [18].

(i) **Analog beamforming**: Without the loss of generality, we assume the l^{th} path component with physical direction of θ_l in (13). Generally , the l^{th} column of the Analog Beamformer F_{RF} in (7) and to obtain the analog beamforming vector a_l:

$$a_l = \frac{1}{N_t}[1, e^{-j2\pi\frac{d}{c}f_c\theta_l}, e^{-j2\pi\frac{2d}{c}f_c\theta_l}, \ldots, e^{-j2\pi\frac{(N_t-1)d}{c}f_c\theta_l}]^T = f_t(2\frac{d}{c}f_c\theta_l) = f_t(\theta_l) \tag{6}$$

Where N_t is number of transmitter antennas, f_c is central frequency, c is speed of light in a vacuum, d is the antenna spacing generally set according to f_c, the central frequency. The analog beamforming vector $a_l = F_{RF}[:, l]$, is used to generate the directional beam to the l^{th} path's physical direction θ_l, which is to be in near optimal [16]. Especially, the analog beamforming technique is to make electromagnetic waves which is transmitted by various antenna elements form an equal phase surface, which is perpendicular to the target physical direction θ_l [23].

(ii) **Hybrid Precoding**: In hybrid precoding, we introduce a baseband precoder(F_{BB}) in addition to the analog beamformer. The overall power constraint is imposed after normalizing F_{BB} so that $||F_{RF}F_{BB}||_F^2 = M$. A wide-

band ray based channel model in (14) is considered, where the m^{th} sub carrier the received signal r_m as

$$r_m = H_m \Sigma_{n=1}^{M} F_{RF} f_n^{BB} s_n + n_m \tag{7}$$

where H_m is the $N_r N_t$ matrix which denotes the channel present in between the m^{th} sub carrier and the AP. The Gaussian noise with corrupting received signal is given by $n_m \sim N(0, \sigma^2 I)$. For processing the received signal y_m, the RF combiner w_m at the m^{th} MS is given by:

$$y_m = w_m^* H_m \Sigma_{n=1}^{M} F_{RF} f_n^{BB} s_n + w_m^* n_m \tag{8}$$

where w_m holds same constraints like RF precoders, that is the constant modulus and quantized angles constraints [18]. However, hybrid precoding is not ideal for capacity and flexibility requirements and can not be used in THz networks due to large array gain losses because of beam split effect [22].

(iii) **Proposed Delay-Phase Precoding (DPP)**: Owing to the draw-

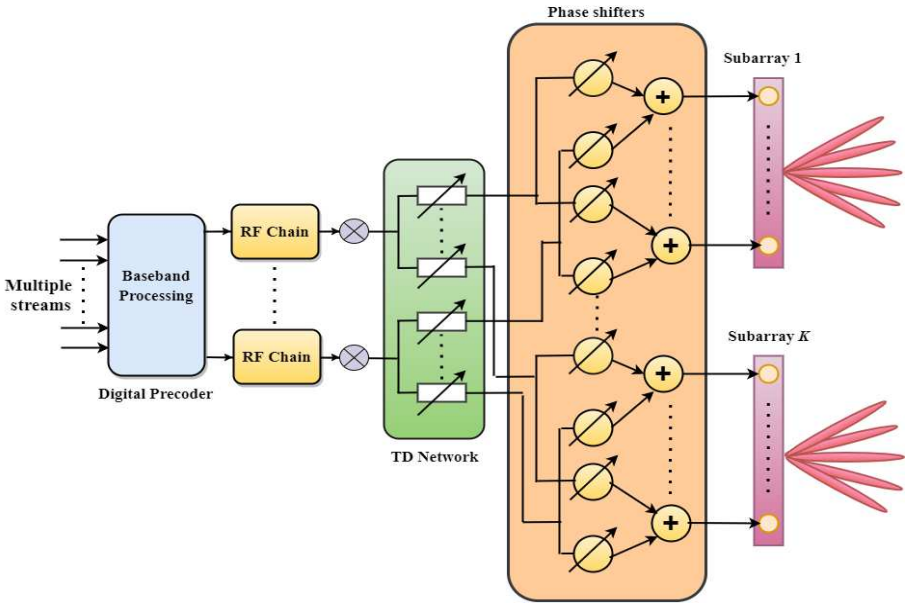

Fig. 5: The proposed DPP network

backs of the aforementioned precoding methods, a newfangled precoding methodology called Delay-phase precoding is proposed [22], [23]. In this technique we consider a conventional hybrid precoding with a THz massive MIMO system. The AP uses N_{RF} radio-frequency chains and N_t-antenna uniform linear array(ULA). By serving an N_r-antenna user, the simultaneous transmission of N_s data streams is done ($N_s = N_r \leq N_{RF} \ll N_t$). The orthogonal frequency

division multiplexing (OFDM) technique is adopted for realizing the reliable wide-band transmission having 'M' sub-carriers. In between the conventional analog beamformer and the digital precoder, a time-delay(TD) network has been introduced . Here the suggested DPP helps to convert the conventional beamformer (phase controlled) into the controlled beamformer with combined delay-phase that is used in the realization of beamforming which is frequency dependent. Every RF chain is linked to 'K' TD elements and every TD element will be linked to '$P_t = N_t/K$' conventional frequency independent phase shifters in a sub connected fashion. Therefore, at m^{th} subcarrier, the received signal is represented as

$$y_m = H_m^H \Sigma_{n=1}^{M} F_{RF_n} A_m^{TD} f_m^{BB} s_m + n_m, \tag{9}$$

where $H_m \in C^{N_t \times N_r}$ represents the m^{th} sub-carrier channel, the analog beamformer provided by the frequency-independent PSs is denoted as $F_{RF_n} \in C^{N_t \times N_{RF}}$ with the form as

$$F_{RF_n} = [F_{RF_{n,1}}, F_{RF_{n,2}}, \ldots, F_{RF_{n,N_{RF}}}] \tag{10}$$

where $F_{RF_{n,l}} = blkdiag([\overline{a_{l,1}}, \overline{a_{l,2}}, \ldots \overline{a_{l,K}}])$ represents the analog beamformer that is accomplished by the PSs linked to the l^{th} RF chain through TDs, and $A_m^{TD} \in C^{KN_{RF} \times N_{RF}}$ represents the frequency-dependent phase shifts that is accomplished by TD network, that satisfies:

$$A_m^{TD} = blkdiag([e^{-j2\pi f_m t_1}, e^{-j2\pi f_m t_2}, \ldots, e^{-j2\pi f_m t_{N_{RF}}}]) \tag{11}$$

The baseband precoder is denoted by $F_{BB_m} \in C^{N_{RF} \times N_s}$ at the m^{th} subcarrier and an additive white Gaussian noise (AWGN) is represented by $n_u \in C^{N_r \times 1}$ at the m^{th} sub-carrier [22].

4.1 Massive MIMO Channel Model

A wide band 'ray-based' channel model is considered for the THz channel [22]. By denoting 'f' as bandwidth and 'f_c' as central frequency, the m^{th} sub-carrier frequency is represented as follows:

$$f_m = f_c + \frac{f}{M}(m - 1 - \frac{M-1}{2}), m = 1, 2, \ldots, M. \tag{12}$$

For m^{th} sub-carrier, the channel is given as

$$H_m = \Sigma_{l=1}^{L} g_l e^{j2\pi\tau_l f_m} f_t(\theta_{l,m}) f_r(\phi_{l,m})^H \tag{13}$$

The total number of resolvable paths are represented by 'L', τ_l and g_l denotes the path delay and path gain of the l^{th} path, $\theta_{l,m}, \phi_{l,m} \in [-1, 1]$ represent the spatial direction of the transmitter and the receiver of the l^{th} path and m^{th} sub-carrier, respectively, and $f_t(\theta_{l,m}), f_r(\phi_{l,m})$ denotes the array responses in the transmitter and the receiver.

For example, $f_t(\theta_{l,m})$ is represented as follows:

$$f_t(\theta_{l,m}) = \frac{1}{\sqrt{N_t}}[1, e^{j\pi\theta_{l,m}}, e^{j\pi\theta_{2l,m}}, \ldots, e^{j\pi(N_t-1)\theta_{l,m}}]^T \tag{14}$$

$$f_t(\phi_{l,m}) = \frac{1}{\sqrt{N_r}}[1, e^{j\pi\phi_{l,m}}, e^{j\pi\phi_{2l,m}}, \ldots, e^{j\pi(N_r-1)\phi_{l,m}}]^T \tag{15}$$

The direction of the paths in the spatial domain is the spatial direction that is determined by the subcarrier frequency and the physical propagation direction. For example, for the transmitter spatial direction, $\theta_{l,m} = 2d\frac{f_m}{c}\sin\gamma_l$, where $\gamma_l \in$[-$\pi/2, \pi/2$] denotes the physical propagation direction of the l^{th} path, 'd' denotes the constant antenna spacing having $d = \frac{c}{2f_c}$ and 'c' represents the speed of the light.

5 Design Approach

To accomplish three precoding techniques, an effective algorithm is proposed. The essence of this proposed algorithm lies in dividing the precoder calculation into three stages. To maximize the desired signal power, the analog beamformer is designed in stage-1 and in the time delays are added to it in stage-2. In the third and last stage, the design of digital(baseband) precoder using the equivalent channel is done.

Algorithm 1: Wideband Precoding for Thz Massive MIMO [22]

Inputs: Spatial directions $\theta_{l,c}$,Channel H_m;
Outputs: $F_{RF_u}, F_{BB_m}, A_m^{TD}$;
First stage: Analog Beamforming
1. **for** l $\in \{1, 2, \ldots,$N$_{RF}$ $\}$ **do**
2. Generate $F_{RF_{u,l}}$ by $[\widetilde{a}_{l,1}, \widetilde{a}_{l,2}, \ldots, \widetilde{a}_{l,K}]^T = f_t(\theta_{l,c})$;
3: **end for**
4: $F_{RF_u} = [F_{RF_{u,1}}, F_{RF_{u,2}}, \ldots, F_{RF_{u,N_{RF}}}]$;
Second stage: Hybrid Precoding
5: $H_{m,eq} = H_m^H F_{RF_u} A_M^{TD}$;
6: $F_{BB_m} = \mu V_{m,eq,[:,1:N_{RF}]}$, $H_{m,eq} = U_{m,eq}\Sigma_{m,eq}V_{m,eq}^H$;
7: **end for**
Third stage: Delay-Phase Precoding
8: **for** l $\in \{1, 2, \ldots,$N$_{RF}$ $\}$ **do**
9: s$_l = -\frac{P\theta_{l,c}}{2}$;
10: $t_{l,i} = \begin{cases} (K-1-i)\lfloor s_l \rceil T_c, \theta_{l,c} > 0 \\ i\lfloor s_l \rceil T_c, \theta_{l,c} \leq 0 \end{cases}$;
11: $t_l = [t_{l,1}, t_{l,2}, \ldots, t_{l,K}]$;
12: **end for**
13: **for** $m \in \{1, 2, \ldots, M\}$ **do**
14: $A_m^{TD} =$ diag($[e^{-j2\pi f_m t}, \ldots, e^{-j2\pi f_m t_{N_{RF}}}]$);
15: **end for**
16: **return** F_{RF_u}, F_{BB_m} *and* A_m^{TD}.

Table 2: Precoding Techniques

Technique	$Sumrate(R)$
Analog Beamforming	$\frac{\frac{P_t}{M}\lvert w_m^H H_m f_m^{RF}\rvert^2}{\frac{P_t}{M}\Sigma_{n\neq m}\lvert w_m^H H_m f_n^{RF}\rvert^2+\sigma_m^2}$
Hybrid Precoding	$\frac{\frac{P_t}{M}\lvert w_m^H H_m F_{RF} f_m^{BB}\rvert^2}{\frac{P_t}{M}\Sigma_{n\neq m}\lvert w_m^H H_m F_{RF} f_n^{BB}\rvert^2+\sigma_m^2}$
Delay-Phase Precoding	$\frac{1}{M}\Sigma_{m=1}^{M} log_2(\lvert I_{N_s}+\frac{P_t}{N_s\sigma_m^2}H_m F_{RF_m} F_{BB_m} F_{BB_m}^H F_{RF_m}^H H_m^H\rvert)$

In this algorithm, the analog precoder for the l^{th} beam $F_{RF_{u,l}}$ is estimated initially in the step 2 for generating the beams in the spatial direction $\theta_{l,c}$. After that the analog beamformer F_{RF_u} is generated in step 4. The time delays by 'K' TD elements have been generated in subsequent steps 6, 7 and 8, where the direction of beams are altered from $\theta_{l,c}$ to $\theta_{l,m}$ at the frequency f_m. Next in step 11, the analog beamformer with the time delay A_m^{TD} is generated. Ultimately, in step 12 and 13, the digital precoder F_{BB_m} is estimated depending upon the equivalent channel $H_{m,eq}$ by conventional singular value decomposition precoding method. From the Algorithm 1, the DPP achieves near-optimal achievable rate, as every beam is aligned with the spatial direction at all the sub-carriers by time delays. This will be further verified by using the results obtained from the simulation.

5.1 Performance Evaluation

The system's performance is calculated by using SE [(bits/s)/Hz] for every user. It is evaluated by (17) where the $SINR_m$ for the considered precoding methods are tabulated under Table 2. The system's sum rate R (bits/s) is given by (18)

$$SE_m = log_2(1 + SINR_m) \tag{16}$$

$$R = \Sigma_{m=1}^{M}(BW_m \times SE_m) \tag{17}$$

where BW_m is the allocation of bandwidth for each user. Equal allocation of power is considered, where the total power is allocated uniformly for the users that is observed in the Table 2.

6 Simulation results and discussion

For comparing the achievable sum-rate of three different precoding methodologies along with the optimal fully-digital precoding, the simulation results are provided. A multi-user single cell THz system is considered 5 GHz bandwidth at 0.14 THz of carrier frequency. The AP equips a 256-element ULA for

Table 3: Simulation Parameters for Precoding Techniques

The number of the AP antennas N_t	256
The number of the user antennas N_r	1
Number of channel paths L	4
The central frequency f_c	0.14 THz
The bandwidth B	5 GHz
The number of the subcarriers M	128
The number of RF chains N_{RF}	4
The number of TD elements K	4,16
Physical directions of the paths $\overline{\theta_l}$, $\overline{\phi_l}$	$\mathcal{U}[\pi/2, \pi/2]$
The transmission SNR P_t/σ^2	-20 $\sim$ 15dB

serving multiple users. The system parameters are shown in Table 3. From the Fig 6 & 7, the proposed Delay-phase precoding's achievable rate performance, Analog Beamforming and Hybrid precoding and is compared for the values of number of time delayers, K=4 and K=16 also it can be inferred that this DPP methodology outperforms other methodologies and attains 97% performance of the standard method, the optimal unconstrained full-digital precoding, due to the joint control of delay-phase.

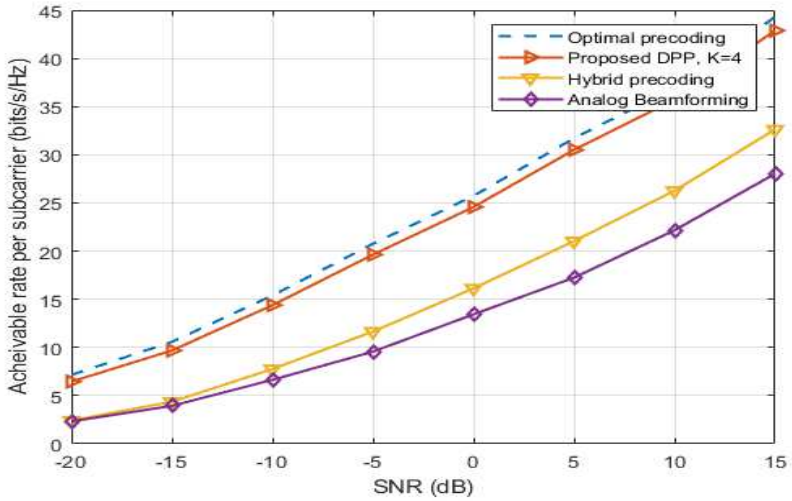

Fig. 6: Achievable rate performance comparison for 4 time delayers (K=4)

Fig. 6 depicts the achievable sum-rate performance for different precoding techniques when the number of time delayers are set to 4. From the Fig. 6, the optimal fully-digital precoding's performance is been compared with the hybrid precoding structure with PSs, which is suffering from severe loss in the

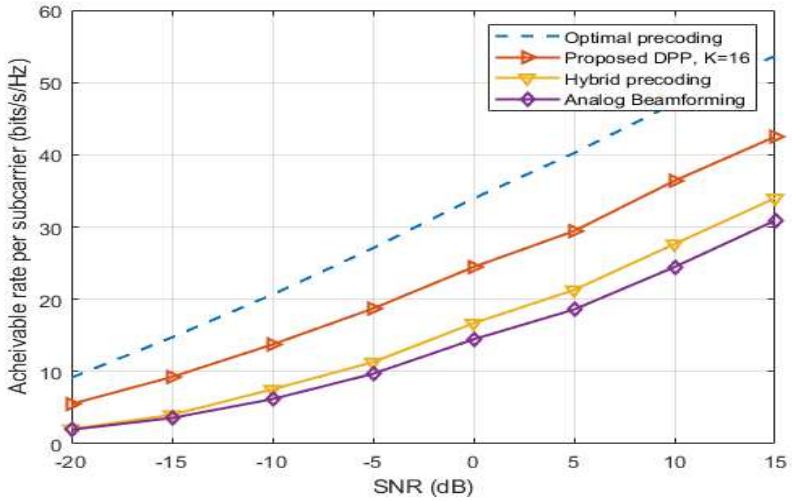

Fig. 7: Achievable rate performance comparison for 16 time delayers (K=16)

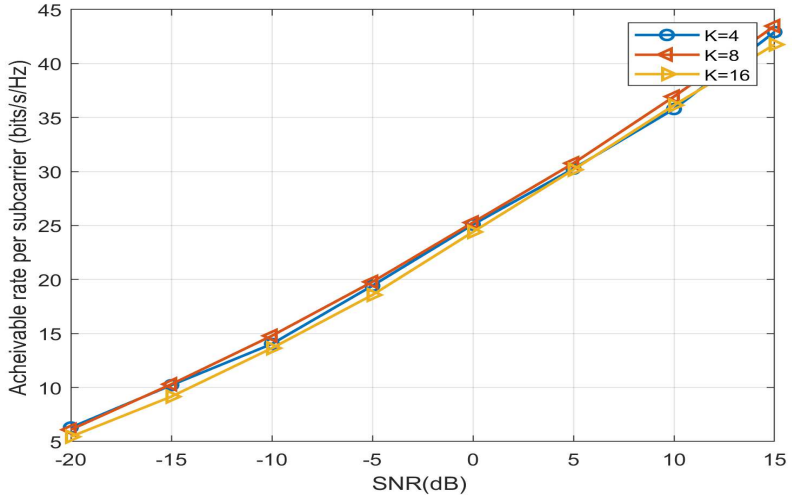

Fig. 8: The rate performance comparison for different number of time delayers

achievable sum-rate. It is due to the fact that they are not having capability to deal with the beam split effect. Conversely, hybrid precoding technique with TDs yield high performance. For the K= 4 the proposed DPP having achievable sum-rate of 42.86 bits/s/Hz near to optimal precoding (97%) which is 44.12 bits/s/Hz from Table 4. Similarly, the proposed DPP outperforms

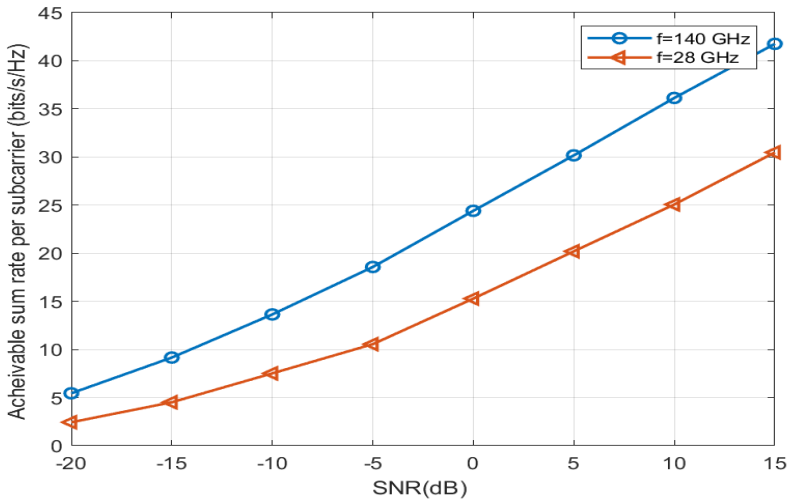

Fig. 9: The rate performance comparison for THz channel and mmWave channel

Table 4: Comparison of various precoding algorithms spectral efficiency (K=4) at SNR= 15dB

Precoding method	No. of Antenna	SE (bits/s/Hz)
Optimal Precoding	256	44.12
Analog Beamforming	256	27.78
Hybrid Precoding	256	32.65
Proposed DPP	256	42.92

Table 5: Comparison of various precoding algorithms spectral efficiency(K=16) at SNR= 15dB

Precoding method	No. of Antenna	SE (bits/s/Hz)
Optimal Precoding	256	53.7
Analog Beamforming	256	30.89
Hybrid Precoding	256	33.99
Proposed DPP	256	41.76

other methods like analog beamforming and hybrid precoding as per the Table 5 and Fig 7.

The proposed Delay-phase precoding network's performance with different number of time delayers has been compared in Fig 8. From the comparison, it is inferred that for the values of K=4 and K=8 are higher than the K=16. Therefore to implement the proposed network, the optimum value of the number of time delayers used in the circuit should be lesser, like K=4 or K=8 than choosing K=16.

Table 6: Comparison of various DPP precoding algorithms spectral efficiency for different time delayers at SNR= 15dB

Precoding method	No. of time delayers(K)	SE (bits/s/Hz)
Proposed DPP	4	42.92
Proposed DPP	8	43.47
Proposed DPP	16	41.76

The proposed Delay-phase precoding network's performance in THz channel and in mmWave channel has been compared in Fig 9. It can be observed that its performance is much better at frequency, f=0.14 THz (sub-THz channel) than at f=28 GHz (mmWave channel). For THz channels, the DPP network is effectively being able to negate the beam split effect caused by the traditional phase-shifters and improve the performance rate substantially whereas in mmWave channel, the proposed DPP network is not able to effectively cancel out the beam squint effect.

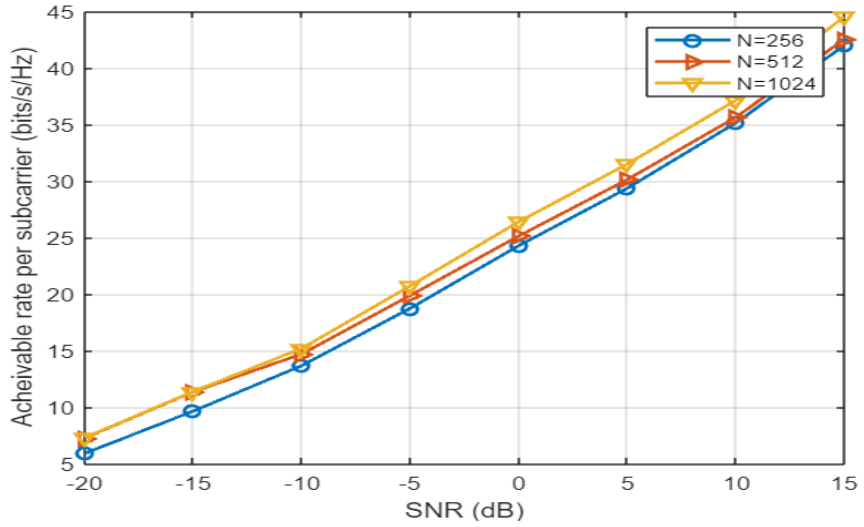

Fig. 10: Comparison of rate performance for different number of antennas

In the Fig 10, the performance of the proposed DPP is compared for various number of AP antennas (N). There is not much difference observed when the value of N changes. Optimal performance is observed at N = 1024. Therefore, the DPP has the capability for solving the achievable rate degradation received by the beam split effect also to achieve more optimal achievable rate performance.

7 Conclusion

This work verified the downlink single cell AP connected to multiple users for the 6G indoor office network deployment scenario and describes the channel model, the antenna properties, and power delay profile analysis employed using NYUSIM Channel Simulation. After that, we proposed a DPP technique where a TD network is being introduced to compensate the beam split effect and compared its performance to Hybrid precoding and Analog beamforming based on traditional frequency-independent phase shifters. From the simulation results and the theoretical analysis, it is observed that this DPP technique is capable to eradicate the beam split effect with more optimal (97%) achievable rate performance. Under DPP Technique, the impacts of the carrier frequency of 28 GHz mmWave and 140 GHz, the number of transmitting antennas and the number of time delayers on the achievable sum rate performance for a single cell multi-user scenario have been compared. This work will be further broadened for multi-cell scenario in future.

Conflict of Interest:

The authors declare that they have no conflict of interest

8 References

1. Z. Zhang, Y. Xiao, Z. Ma, M. Xiao, Z. Ding, X. Lei, G. K. Karagiannidis, and P. Fan, "6G wireless networks: Vision, requirements, architecture, and key technologies," IEEE Veh. Technol. Mag., vol. 14, no. 3, pp. 28–41, Sep. 2019.
2.T. S. Rappaport, Y. Xing, O. Kanhere, S. Ju, A. Madanayake, S. Mandal, A. Alkhateeb, and G. C. Trichopoulos, "Wireless communications and applications above 100 GHz: Opportunities and challenges for 6G and beyond," IEEE Access, vol. 7, pp. 78 729–78 757, Jun. 2019.
3.Mumtaz, S., Jornet, J. M., Aulin, J., Gerstacker, W. H., Dong, X., Ai, B. (2017). Terahertz communication for vehicular networks. IEEE Transactions on Vehicular Technology, 66(7).
4. Akyildiz, I. F., Jornet, J. M., Han, C. (2014). Terahertz band: Next frontier for wireless communications. Physical Communication, 12, 16-32.
5. Lin, C., Li, G. Y. (2016). Energy-efficient design of indoor mmWave and sub-THz systems with antenna arrays. IEEE Transactions on Wireless Communications, 15(7), 4660-4672.
6. Busari, S. A., Mumtaz, S., Al-Rubaye, S., Rodriguez, J. (2018). 5G millimeter-wave mobile broadband: Performance and challenges. IEEE Communications Magazine, 56(6), 137-143.
7. Busari, S. A., Khan, M. A., Huq, K. M. S., Mumtaz, S., Rodriguez, J. (2019). Millimetre-wave massive MIMO for cellular vehicle-to-infrastructure communication. IET Intelligent Transport Systems, 13(6), 983-990.

8. X. Gao, L. Dai, S. Han, C. L. I, and R. W. Heath, "Energy-efficient hybrid analog and digital precoding for mmwave MIMO systems with large antenna arrays," IEEE J. Sel. Areas Commun., vol. 34, no. 4, pp. 998–1009, Apr. 2016.
9. C. Lin and G. Y. Li, "Terahertz communications: An array-of-subarrays solution," IEEE Commun. Mag., vol. 54, no. 12, pp. 124–131, Dec. 2016.
10. C. Han and I. F. Akyildiz, "Distance-aware bandwidth-adaptive resource allocation for wireless systems in the terahertz band," IEEE Trans. THz Sci. Technol., vol. 6, no. 4, pp. 541–553, Jun. 2016.
11.Busari, S. A., Huq, K. M. S., Mumtaz, S., Dai, L., Rodriguez, J. (2017). Millimeter-wave massive MIMO communication for future wireless systems: A survey. IEEE Communications Surveys Tutorials, 20(2), 836-869.
12.Alkhateeb, A., Leus, G., Heath, R. W. (2015). Limited feedback hybrid precoding for multi-user millimeter wave systems. IEEE transactions on wireless communications, 14(11), 6481-6494.
13.Chih-Lin, I. (2017). Seven fundamental rethinking for next-generation wireless communications. APSIPA Transactions on Signal and Information Processing, 6.
14.Huq, K. M. S., Mumtaz, S., Bachmatiuk, J., Rodriguez, J., Wang, X., Aguiar, R. L. (2014). Green HetNet CoMP: Energy efficiency analysis and optimization. IEEE Transactions on Vehicular Technology, 64(10), 4670-4683.
15.Busari, S. A., Huq, K. M. S., Felfel, G., Rodriguez, J. (2018, December). Adaptive resource allocation for energy-efficient millimeter-wave massive MIMO networks. In 2018 IEEE Global Communications Conference (GLOBECOM) (pp. 1-6). IEEE.
16.O. E. Ayach, S. Rajagopal, S. Abu-Surra, Z. Pi, and R. W. Heath, "Spatially sparse precoding in millimeter wave MIMO systems," IEEE Transactions on Wireless Communications., vol. 13, no. 3, pp. 1499–1513, Mar. 2014.
17. B. Wang, F. Gao, S. Jin, H. Lin, G. Y. Li, S. Sun, and T. S. Rappaport, "Spatial-wideband effect in massive MIMO with application in mmwave systems," IEEE Communications Magazine., vol. 56, no. 12, pp. 134–141, Dec. 2018.
18. S. Park, A. Alkhateeb, and R. W. Heath, "Dynamic subarrays for hybrid precoding in wideband mmWave MIMO systems", IEEE Transactions on Wireless communications, vol. 16, no. 5, pp. 2907–2920, May 2017.
19. L. Kong, S. Han, and C. Yang, "Hybrid precoding with rate and coverage constraints for wideband massive MIMO systems," IEEE Transactions on Wireless communications, vol. 17, no. 7, pp. 4634– 4647, Jul. 2018.
20. M. Cai, K. Gao, D. Nie, B. Hochwald, J. N. Laneman, H. Huang, and K. Liu, "Effect of wideband beam squint on codebook design in phased-array wireless systems," in Proc. IEEE Global Communication Conferences, Dec. 2016, pp. 1–6.
21. X. Liu and D. Qiao, "Space-time block coding-based beamforming for beam squint compensation," IEEE Wireless Communication Letters, vol. 8, no. 1, pp. 241–244, Feb. 2019.
22. J. Tan and L. Dai, "Delay-Phase Precoding for THz Massive MIMO with Beam Split," 2019 IEEE Global Communications Conference (GLOBECOM),

Waikoloa, HI, USA, 2019, pp. 1-6, doi: 10.1109/GLOBECOM38437.2019.9014304.
23. Dai, L., Tan, J., Poor, H. V. (2021). Delay-Phase Precoding for Wideband THz Massive MIMO. arXiv preprint arXiv:2102.05211.
24. Sun, S., Rappaport, T. S., Shafi, M., Tang, P., Zhang, J., Smith, P. J. (2018). Propagation models and performance evaluation for 5G millimeter-wave bands. IEEE Transactions on Vehicular Technology, 67(9), 8422-8439.
25. Busari, S. A., Huq, K. M. S., Mumtaz, S., Rodriguez, J. (2019, May). Terahertz massive MIMO for beyond-5G wireless communication. In ICC 2019-2019 IEEE International Conference on Communications (ICC) (pp. 1-6). IEEE.
26. Sun, S., Rappaport, T. S., Thomas, T. A., Ghosh, A., Nguyen, H. C., Kovács, I. Z., ... Partyka, A. (2016). Investigation of prediction accuracy, sensitivity, and parameter stability of large-scale propagation path loss models for 5G wireless communications. IEEE Transactions on Vehicular Technology, 65(5), 2843-2860.
27. Liebe, H. J., Hufford, G. A., Cotton, M. G. (1993). Propagation modeling of moist air and suspended water/ice particles at frequencies below 1000 GHz.
28. Sun, S., MacCartney, G. R., Rappaport, T. S. (2017, May). A novel millimeter-wave channel simulator and applications for 5G wireless communications. In 2017 IEEE International Conference on Communications (ICC) (pp. 1-7). IEEE.
29. Ju, S., Kanhere, O., Xing, Y., Rappaport, T. S. (2019, December). A millimeter-wave channel simulator NYUSIM with spatial consistency and human blockage. In 2019 IEEE Global Communications Conference (GLOBECOM) (pp. 1-6). IEEE.
30. Ju, S., Xing, Y., Kanhere, O., Rappaport, T. S. (2021). Millimeter wave and sub-terahertz spatial statistical channel model for an indoor office building. arXiv preprint arXiv:2103.17127.